Synoptic-Scale Physical Mechanisms Associated With Mei-yu Front: A Numerical Case Study in 1999

by

Nguyen Minh Truong[1a], Vu Thanh Hang[1], Roger A. Pielke Sr.[2],

Christopher L. Castro[3], and Koji Dairaku[4b]

[1]Hanoi University of Science, 334 Nguyen Trai, Thanh Xuan, Hanoi, Vietnam

[2]CIRES, Stadium 255-16, University of Colorado, Boulder, CO 80309

[3]Department of Atmospheric Sciences, University of Arizona

Physics and Atmospheric Sciences Bldg., Rm 520, 1118 East Fourth Street

Tucson, AZ 85721-0081

[4]Storm, Flood, and Landslide Research Department

National Research Institute for Earth Science and Disaster Prevention

3-1 Tennodai Tsukuba Ibaraki 305-0006 Japan

(Submitted for consideration for publication as an article in the *Monthly Weather Review*)

[a]Corresponding author address: Dr. Nguyen Minh Truong, Hanoi University of Science, 334 Nguyen Trai, Thanh Xuan, Hanoi, Vietnam

E-mail: truongnm@vnu.edu.vn

[b]Current affiliation: CIRES, Stadium 255-35, University of Colorado, Boulder, CO 80309

Abstract

The Mei-yu front system occurring from 23 to 27 June 1999 is a typical case and consists of the Mei-yu front and the dewpoint front, which confine a warm core extending from the eastern flank of the Tibetan Plateau to the west of 145°E. To further understand the synoptic-scale physical mechanisms associated with the Mei-yu front system, the present study proposes another insight into the physical significance of x-component relative vorticity whose vertical circulation might tilt isentropic surfaces. Therefore, the x-component relative vorticity equation is used to analyze the Mei-yu frontogenesis and frontolysis since it contains thermodynamic terms which govern tilting isentropic surfaces. The equation diagnoses exhibit that the twisting effect of the planetary vorticity (TEPV) is positive along the Mei-yu front and negative in the dewpoint front region, and tilts isentropic surfaces from south to north in the Mei-yu frontal zone. By contrast, the meridional gradient of the atmospheric buoyancy (MGAB) tilts isentropic surfaces in the opposite direction and maintains negative in the regions where the TEPV is positive and vice versa. Thus, the former plays the role of the Mei-yu frontogenesis meanwhile the latter demonstrates the Mei-yu frontolysis factor. The present simulations also show that weakening of the upper-level jets evidently induces weakening of the Mei-yu front and reduces the amplitude of the East Asia cold trough. Furthermore, the impact can also penetrate into the lower troposphere, proving that the formation and evolution of the Mei-yu front is top-down instead of bottom-up. The stretching effect and the twisting effect of relative vorticity play much minor roles than others in this case study.

1. Introduction

In the latest decades, a large amount of research has been carried out to study the Mei-yu (or Baiu in Japanese) phenomenon since it often accompanies mesoscale disturbances and torrential rain in the East Asian summer monsoon (EASM) region (Shen et al. 2001, Kawatani and Takahashi 2003, Shibagaki and Ninomiya 2005, Ninomiya and Shibagaki 2007). However, the studies may be divided into two common frameworks: the Mei-yu season diagnostic and the Mei-yu front diagnostic framework. For the Mei-yu season diagnostic framework, for example, Sampe and Xie (2010) diagnosed the large-scale environment favorable for the Meiyu-Baiu season and found a close relation between the warm advection and upward motion, indicating the importance of the warm advection for the Meiyu-Baiu formation. Besides, they proposed a hypothesis that the externally induced ascent helps to trigger convection by lifting air parcels, which in turn produces a positive feedback for the Meiyu-Baiu. Kawatani and Takahashi (2003) analyzed the characteristics of large-scale circulations and the configurations of numerical experiments, which could favor simulation of the Baiu front and the Baiu precipitation. Wang et al. (2003) used a highly resolved regional climate model to simulate precipitation in the Mei-yu season from 26 April to 31 August 1998. Their 4-month simulations showed that rainfall associated with the Mei-yu front over the Yangtze River basin (26°-32°N, 110°-122°E) was less convective. Conversely, convective rainfall dominated in south China.

For the Mei-yu front diagnostic framework, abundant research focuses on principal weather systems associated with the Mei-yu front. For example, in 1998, the year after the strongest 1997/98 El Niño event in the 20th century, the Mei-yu front and accompanying weather disturbances caused severe flooding in the Yangtze River basin (Shen et al. 2001, Wang et al. 2003, Qian et al. 2004) and have, therefore, received a lot of attention. Chien et al. (2002) intensively verified the precipitation forecast skill of the MM5 model and

exhibited that during the Mei-yu season in 1998, many mesoscale convective systems (MCS) developed along the front and moved toward Taiwan. Zhang et al. (2003) also used MM5 to depict conditions for the formation of mesoscale features embedded in a mature MCS, such as lower-level jet, upper-level jet, mesolow, and mesohigh etc. Chen et al. (2006) investigated the internal structures and evolution of the Mei-yu front, and analyzed mechanisms producing lower-level jets, their intensification, and the retreat of the Mei-yu front near Taiwan. In their study, the potential vorticity generated and latent heat released by MCS, along with the adjustment to geostrophic balance, were emphasized as major mechanisms.

So far, the Mei-yu studies have recognized the important roles of the Tibetan Plateau, moisture sources, and western Pacific subtropical high (WPSH). Yoshikane et al. (2001) conducted numerical experiments and concluded that the Tibetan Plateau and mountains could significantly affect the Baiu front location, lower- and upper-level jets, and Baiu precipitation but the fundamental structure of the front could be reproduced without any orography. Qian et al. (2004) demonstrated that the moisture flux from the Bay of Bengal played an essential role in Mei-yu precipitation in 1998. The WPSH location might be important in that it would decide where moisture comes from, the South China Sea or Bay of Bengal (Cho and Chen 1995, Shen et al. 2001, Ninomiya and Shibagaki 2007, Sampe and Xie 2010). However, all of the above studies did not explicitly figure out the synoptic-scale physical mechanisms associated with any particular Mei-yu front since they used subjective analyses of the model output fields instead of using analytical relations which are inherently dynamic.

Chen et al. (2003, 2008) used the conserved Ertel's potential vorticity (PV) to diagnose two Mei-yu front cases in 1990 and 2003. Unfortunately, in diabatic heating situations (certainly the case of a Mei-yu front with strong convection), the PV is no longer

conserved (Holton 2004, Chen et al. 2008), while the use of piecewise PV inversion techniques (as well as the complete PV equation) is complicated to interpret physical mechanisms. Another method diagnosing frontogenesis is the use of frontogenetical function. For example, Zhou et al. (2004) used frontogenetical function to diagnose the formation of a typical Mei-yu front system in the La Niña year 1999, including the Mei-yu and dewpoint front. It is unfortunate that the function is a purely kinematic approach (Bluestein 1993, Chen et al. 2007) which can not describe some major physical processes such as the transport by air parcels, development of transverse circulation, and upper-level front (Chen et al. 2007). As cautioned by Chen et al. (2007), "one needs to be cautious in the interpretation of frontogenetical function results because of the above limitations, especially in frontal movement and evolution." In other words, starting with definition formulas containing the gradient of potential temperature, the mathematic manipulations developed might then lead to relations showing outward appearance without addressing the inward essence of frontogenesis. Therefore, a dynamic approach is desirable to understand the large-scale dynamic mechanisms which help to anchor the Mei-yu front as proposed by Sampe and Xie (2010). Along with vertical relative vorticity, the horizontal vorticity equations are useful prognostic tools (Jung and Arakawa 2008). However, in the EASM and Mei-yu studies, most attention was paid to the vertical component (Chen and Chang 1980, Wang 1987, Chang et al. 2000, Chen et al. 2003), although the meridional streamline might be favorable for the synoptic-scale horizontal vorticity in Mei-yu regions (Lau et al. 1988, Chang et al. 2000, Chen et al. 2008, Sampe and Xie 2010). In such circumstance, the present study aims at reproducing synoptic-scale physical mechanisms for the formation and evolution of the Mei-yu front system by a case study in 1999. In the next section, the x-component relative vorticity (XRV) equation is given with physical significances. Model configuration and data are described in Section 3 and numerical simulations are given in

Section 4. Summary and concluding remarks are presented in Section 5.

2. XRV equation and physical significance

The motives for using the XRV equation to clarify mechanisms for the formation and evolution of the Mei-yu front system derive from the evidence found that: 1) according to the conceptual model of the Mei-yu/Baiu front by Ninomiya and Shibagaki (2007), at upper levels there is maximum wind airflow running along the northern and southern flanks of the Tibetan Plateau, which may then extend northeastward to Japan. 2) the Mei-yu front is usually quasi-stationary, originates in south China or the Yangtze River basin, and also frequently extends northeastward to Japan. Thus, the maximum wind airflow is expected to have a close relation with the Mei-yu front (Kawatani and Takahashi 2003, Sampe and Xie 2010). If so, thermodynamic properties accompanying the maximum wind airflow must be taken into account to depict the synoptic-scale physical mechanisms associated with a particular Mei-yu front system. Of those the XRV might be an important one.

As conventional, the x-, y-, and z-component of relative vorticity are respectively defined by

$$\xi \eta \zeta = \frac{\partial w}{\partial y} - \frac{\partial v}{\partial z}, \quad \eta = \frac{\partial u}{\partial z} - \frac{\partial w}{\partial x}, \quad \zeta = \frac{\partial v}{\partial x} - \frac{\partial u}{\partial y} \tag{1}$$

Using two equations of meridional and vertical wind without friction, one may receive the XRV equation

$$\frac{d\xi}{dt} = -\xi\left(\frac{\partial u}{\partial x}\right) - \eta\left(\frac{\partial v}{\partial x}\right) - \zeta\left(\frac{\partial w}{\partial x}\right) + \frac{\partial B}{\partial y}\frac{\partial \alpha}{\partial z} - \frac{\partial B}{\partial z}\frac{\partial \alpha}{\partial y} + f\left(\frac{\partial v}{\partial x}\right) - \beta v$$

or

$$\frac{d\xi}{dt} = -\xi\left(\frac{\partial u}{\partial x}\right) - \eta\left(\frac{\partial v}{\partial x}\right) - \zeta\left(\frac{\partial w}{\partial x}\right) + \left(\frac{\partial B}{\partial y}\frac{\partial \alpha}{\partial z} - \frac{\partial B}{\partial z}\frac{\partial \alpha}{\partial y}\right) + f\left(\frac{\partial v}{\partial x}\right) - \beta v \tag{2}$$

Here *u*, *v*, and *w* are the x-, y-, and z-component of velocity, respectively; $B = g\frac{\theta_v'}{\theta_0}$ is the buoyancy. θ_v' is the virtual potential temperature perturbation, θ_0 is the reference state potential temperature which is at hydrostatic state, and *f* is the Coriolis parameter. On the right-hand side of Eq. (2), the first term describes the stretching effect (SERV), the second term is the twisting effect of relative vorticity (TERV), the third term is the twisting effect of the planetary vorticity (TEPV), and the last one represents the meridional gradient of the atmospheric buoyancy (MGAB).

Equation (2) states that ξ might be nonconserved. In zonal jet regions, strong vertical shear of zonal wind twists the planetary vorticity and favors positive XRV which, in turn, supports ascending (descending) motion to the north (south) of jet, where the air is expected cooler (warmer). As a result, the TEPV tends to tilt isentropic surfaces and make the atmosphere less stably stratified. By contrast, the Earth's gravity trends toward forcing cooler air to sink to the north and warmer air to rise to the south of jet, i.e., negative MGAB tilts isentropic surfaces in the opposite direction (Fig. 1). The effects of the TEPV and MGAB are similar to the tilting effects described in Figure 2.11 by Bluestein (1993). Thus, these two effects are presumably opposite and a relative balance between them might keep the warmer air stationary to the south and cooler air to the north of jet and make fronts likely formed. Any deviation from such balance might lead to front strengthening or weakening. If ξ is positive, the frontal convergent circulation makes the SERV positive. The sign of the TERV depends on the spatial distribution of velocity components, however, this term is not expected of a dominant factor in the Mei-yu front circulation. In short, if an air parcel increases (decreases) its Lagrangian ξ while moving downstream, the environment across its pathway downstream must be conducted so that the right-hand side of Eq. (2) remains positive (negative), which might favor frontogenesis (frontolysis). Note

that 1) equation (2) is an unique analytical expression containing the linear term of the MGAB, which can presumably depict the Mei-yu front system as it appears in nature (the Ertel's potential vorticity and frontogenetical function are nonlinear to the gradients of potential temperature). In other words, unlike the traditional approach using the horizontal gradient of potential temperature, the present study uses the MGAB to detect fronts, since it is known that thermodynamic properties change suddenly across the frontal zones. Imagine that the MGAB tends to approach zero while making the atmosphere stably stratified, i.e., frontolysis effect, but its presence itself represents the presence of front. 2) The right-hand side of Eq. (2) must strictly be bounded two-sidedly about zero so that ξ cannot approach infinite. Therefore, there might be mechanisms in destructing the air parcels' XRV (sink terms), including the meridional change of the atmospheric buoyancy, which expectedly indicates the Mei-yu front system and induces convection in favorable conditions.

If assume ξ conserved then Eq. (2) reduces to

$$\frac{\partial}{\partial t}\left(\frac{\partial v}{\partial x}-\frac{\partial u}{\partial y}+f\right)=-\left(\frac{\partial u}{\partial x}+\frac{\partial v}{\partial y}\right)\frac{\partial B}{\partial z}+\left(\frac{\partial v}{\partial z}\frac{\partial B}{\partial x}-\frac{\partial u}{\partial z}\frac{\partial B}{\partial y}\right) \tag{3}$$

which describes the balance between the vorticity terms, TEPV and MGAB.

3. Model configuration and data

In the present study, the Regional Atmospheric Modeling System (RAMS version 4.4) is used to simulate the Mei-yu front system from 0000 UTC 23 to 0000 UTC 27 June 1999. The simulation period is chosen similar to that used by Zhou et al. (2004). The initial conditions for the RAMS simulations are specified by using the NCEP-NCAR Reanalysis data (Kalnay et al. 1996). These data consist of horizontal wind, temperature, relative humidity, and geopotential height on 17 isobaric surfaces with a horizontal grid interval of

2.5° × 2.5°. The boundary conditions are updated every 6 h using the same data source. A Barnes objective analysis scheme is used to interpolate the initial data onto the model grids. The interpolation operator for the updated lateral boundary conditions is implemented using a quadratic function. The sea surface temperature (SST) data is the weekly SST given by NOAA (Reynolds et al. 2002).

Centered at 35°N-108°E, the domain of the present study respectively includes 207 × 161 grid points in the zonal and meridional direction with a grid spacing of 45 km. As shown in Fig. 2 the model topography may reach more than 5500 m above mean sea level (MSL) over the Tibetan Plateau. The model grid contains 30 levels and is vertically stretched with a 1.15 ratio. The lowest grid spacing is 100 m and the maximum vertical grid spacing is set to 1200 m. The convective parameterization scheme (CPS) is the modified Kain-Fritsch scheme described by Truong et al. (2009) where a new trigger function, closure assumption, and equation to compute updraft velocity are developed. The CPS is activated every 5 minutes. The explicit microphysical representation of resolvable precipitation is the scheme developed by Walko et al. (1995). The model configuration and experiments are summarized in Table 1 where Ctrl and Jmod are the control and jet-modification run (see Section 4), respectively. In the following sections the Ctrl run is discussed, otherwise the Jmod run is mentioned.

4. Numerical simulations and discussions

a. The Mei-yu front evolution

To be consistent with Eq. (2), virtual potential temperature is used to represent the Mei-yu front system instead of equivalent potential temperature as in some other studies, although the equivalent potential temperature should make the fronts look stronger. Figure 3 illustrates the evolution of the Mei-yu front system at 700 hPa from 23 to 26 June 1999 at

1200 UTC. At the early stage, a hot low occurs immediately to the southeast of the Tibetan Plateau where southwest wind is maximum and blows toward Japan (Fig. 3a). At the same time, a cold trough locates west of the Korean peninsula. As time elapses, the cold trough comes out of the domain to the east and the Mei-yu front system starts to develop toward Japan (Fig. 3b,c,d), including two branches: the Mei-yu front and the dewpoint front (Zhou et al. 2004). The Mei-yu front extends from about 32°N-103°E to 36°N-145°E meanwhile the dewpoint front clearly originates from 21°N-110°E, extends northeastward and merges into the Mei-yu front (Fig. 3c), creating the Mei-yu front system. As usual, the meridional gradient of virtual potential temperature along the dewpoint front is significantly weaker than along the Mei-yu front (Zhou et al. 2004). Except the hot low immediately to the southeast of the Tibetan Plateau, there are mesoscale hot centers or disturbances confined by the Mei-yu front system, which are aligned along the maximum westerly wind airflows. The development process of the Mei-yu front over Japan accompanies the eastward propagation of the cold trough and mesoscale disturbances, and the presence of midlatitude westerly wind (Ninomiya and Shibagaki 2007, Sampe and Xie 2010). That is why the hot low is often called the southwest vortex (of the Mei-yu front) which presumably generates mesoscale disturbances propagating along the fronts (Sampe and Xie 2010). It is also found that the development process of the Mei-yu front is out of phase between the sections in China and over Japan while southerly wind develops and blows throughout China. This evolution follows closely with the NCEP-NCAR Reanalysis data (not shown).

At 300 hPa the cold trough locates west of the Korean peninsula along with a ridge to the northwest of Japan to create a short thermal wave across the East Asia shoreline at 1200 UTC 23 June (Fig. 4a). On the next days, the thermal wave propagates eastward and the Mei-yu front starts to develop over Japan and adjacent seas (Fig. 4b,c,d), similar to the previous mentions. Note that the front-like section along the northern flank of the Tibetan

Plateau may not be called “Mei-yu”, however, in the present study “Mei-yu” is used for simplicity. At this level, the Mei-yu front is much stronger, by contrast, the dewpoint front almost disappears (Zhou et al. 2004). Along the dewpoint frontal zone, wind vector remains very light on the first two days, but is accelerated on the last two days. The Tibetan high circulation develops by 1200 UTC 25 June when the 700-hPa Mei-yu front system becomes mature over the western Pacific and weakens in China (Fig. 3c). In general the pattern at 300 hPa is similar to 700-hPa pattern along the Mei-yu frontal zone except the presence of the Tibetan high circulation in China. It is evident from the figures that development of the Mei-yu front coincides with the development of the maximum wind airflow (upper-level jets) moving along the front. Comparison between Figs. 3 and 4 indicates that the front is tilted to the north with height. The Mei-yu front system weakens on 26 June (Figs. 3d, 4d). Basically, the Mei-yu thermal patterns closely follow a typical structure in this case study as they show a clear warm core which extends from the eastern flank of the Tibetan Plateau to the west of 145°E. In the EASM studies, terminology “warm core” is usually used to indicate the hot centers which are bounded by the Mei-yu and dewpoint front at lower levels and are associated with the Tibetan high at higher levels (Chen et al. 2003, 2008; Yanai and Wu 2006; Yihui and Chan 2005). The XRV distribution indicates that the Mei-yu front can neither develop nor last long where the XRV is negative and vice versa. For the quasi-stationary Mei-yu sections, the XRV is nearly equal to zero, showing a balance state as given by Eq. (3) (not shown).

b. The Mei-yu precipitation

On the first day, the model gives a heavy rainfall band along the southern flank of the Himalayas (similar to Yoshikane et al. 2001), an extensive heavy rainfall region over all Burma, and a heavy rainfall region in southern and central China, which is associated

with the Mei-yu front system. A local maximum center can be found in the Yangtze River valley (30°N-105°E) and another extensive heavy rainfall region covering all Japan and the Korean peninsula (Fig. 5a) might be induced by the wind convergence to the southeast of the cold trough (Fig. 3a). Afterwards, the heavy rainfall regions extend northward in China, southward to the Indochina peninsula, and eastward over Japan and adjacent seas, accompanying with development of the Mei-yu front. Distribution of the simulated precipitation shows good agreement with Zhou et al. (2004) and TRMM data (not shown).

It is interesting that although the simulated precipitation spreads over all East Asian regions on the first two days, it appears much narrower and lighter over India and the tropical Indian Ocean (Fig. 5a,b). The reason for this might be the convergence to the south of the Tibetan high at upper levels (not shown), similar to Shen et al. (2001), which in turn might cause synoptic-scale subsidence suppressing convection over these regions. Thus, this case study is a good example suggesting again that the East Asian summer monsoon, which can be classified as a subtropical monsoon system, is not a simple extension to the east of the South Asian summer monsoon (Yihui and Chan 2005).

c. The XRV equation diagnoses

Figure 6 represents the MGAB at 700 hPa from 23 to 26 June at 1200 UTC. When the Mei-yu front system starts to develop, this term has positive increasing values in the hot low and along the dewpoint front but remains negative in the Mei-yu front region (Fig. 6a,b), appearing consistent with the warm-core structure as mentioned. At the latter stages, the MGAB prevails negative and distributes consistently with the Mei-yu front system development, that is, it decays in China but zonally broadens over Japan and adjacent seas (Fig. 6c,d).

The TEPV distributions at 700 hPa are given in Fig. 7. Opposite to the MGAB, the

TEPV is positive and generally dominates with larger magnitudes in the Mei-yu front regions (Fig. 7a,b). Thus, positive zonal wind actually increases quickly with height along the fronts (e.g., Figs. 3, 4) and this itself supports the fronts' formation and evolution as explained by Fig. 1. By contrast, the MGAB dominates when sections of the front weaken in China on 25 June (Figs. 6c, 7c) and later over southern Japan (Figs. 6d, 7d), showing the frontolysis effect of the MGAB. Along the dewpoint front region, the TEPV is negative and dominates over the MGAB while the front develops (Fig. 7b,c). An opposite interpretation can be given for the last day (Fig. 7d). The SERV and TERV are much smaller than others in this case study (not shown).

At 300 hPa, the distribution of the MGAB follows a similar pattern to 700 hPa except in the dewpoint front regions where it almost vanishes (Fig. 8). This means the Mei-yu front contains larger thermal deviation from the hydrostatic state than the dewpoint front in the whole troposphere, which requires a large-scale dynamic source to maintain this state. As expected, the MGAB can be used to detect the fronts as it becomes stronger and smoother with height in the Mei-yu frontal zone. Figure 9 shows the pattern of the TEPV at this level, which again dominates over the MGAB in the Eurasian continent and offshore along the Mei-yu front (Fig. 9a,b,c) except over the Korean peninsula, Japan and adjacent seas when the front weakens (Fig. 9d). At this point of view, the TEPV is the required condition for the fronts to form and develop with height (i.e., the dewpoint front weakens with height). The common magnitudes of the terms in the XRV equation are summarized in Table 2. In terms of Lagrangian χ, the TEPV plays the role of a source term meanwhile the MGAB manifests the role of a sink term and the balance between them would decide if the fronts could be formed along the upper-level jets' trajectory.

d. The role of the upper-level jets

In the above subsections, the upper-level jet appears as a key factor. Moreover, for any scalar, its gradient is generally larger near its source. If so, the source of the Mei-yu front presumably locates at higher levels. To clarify, an experiment (Jmod) is set up where wind speed is reduced by

$$if\ |V_{thea}| \geq 45 \quad 45 + 0.3 * (|V_{thea}| - 45) \qquad (4)$$

Equation (4) ensures that the only portion of wind speed exceeding 45 m s^{-1} is reduced by 70%, so the wind field is only modified in the layer from about 500 hPa upward, although it should remain smooth with the same direction.

Similar to Fig. 4 the evolution of the Mei-yu front system at 300 hPa is given in Fig. 10 where the upper-level jets are weakened according to Eq. (4). In general the Mei-yu thermal pattern is kept the same until 1200 UTC 23 June when the upper-level jets do not yet develop (Figs. 10a, 4a). By 1200 UTC 24 June, a subtle difference can be seen to the east of the East Asia shoreline with a little weakening of the Mei-yu front (Figs. 10b, 4b). Note that the cross-front scale is much smaller than the domain. On the next day when the upper-level jets fully develop, the Mei-yu front is much weakened along with a decrease in the amplitude of the cold trough over the Korean peninsula and northern Japan (Figs. 10c, 4c; and 10d, 4d). The primary reason for this is that Eq. (4) could reduce the vertical shear of zonal wind as well as the TEPV, which in turn leads to less tilting isentropic surfaces (more mentioned below) and the reduction of the MGAB (not shown). Therefore, it should be concluded that the upper-level jets' development is the direct cause of the Mei-yu front and cold trough strengthening.

Figure 11 is plotted to show the difference in 300-hPa virtual potential temperature between the Ctrl and Jmod experiment from 23 to 26 June 1999 at 1200 UTC. It is apparent that the difference does not occur until 1200 UTC 23 June (Fig. 11a) when the upper-level jets do not yet develop. Subsequent to the upper-level jets' development, the

Mei-yu front is “cooling” in the front section over the Korean peninsula and northern Japan due to the decrease in the amplitude of the cold trough in the Jmod experiment (Fig. 11b,c,d). The “cooling” effect is strongest when the front reaches maturity on 25 June (Fig. 11c). This phenomenon is consistent with the explanation illustrated by Fig. 1, that is, stronger TEPV forces the atmosphere less stably stratified by more tilting isentropic surfaces but when the upper-level jets are weakened, the MGAB is still present and persistently stabilizes the atmosphere by tilting isentropic surfaces in the opposite direction.

Downward to 700 hPa, the Mei-yu thermal pattern is almost kept the same until 1200 UTC 24 June (Fig. 12a,b). Around 1200 UTC 25 June, the Mei-yu front is weakened offshore along the eastern boundary of Japan in the Jmod experiment (Fig. 12c). At the same time, a “warming” center locates on the place of the mesoscale hot center in Fig. 3c. On the last day, the “warming” center propagates eastward to the south of Japan (Fig. 12d), consistent with the mesoscale hot center in Fig. 3d. It is worthy to note that the “warming” centers are not found at upper levels (e.g., Fig 11) and this, therefore, suggests that the upper-level jets excite and steer the mesoscale disturbances propagating eastward (similar to Sampe and Xie (2010)). Recall that Eq. (4) modifies the wind field in the layer from about 500 hPa upward; however, the impact on the front’s structure is evident at 700 hPa. Besides, the impact is lessened downwards with an obvious time lag. This proves that the formation and evolution process of the Mei-yu front is top-down instead of bottom-up.

e. The meridional-vertical cross sections

To further investigate the evolution of the Mei-yu thermodynamic pattern, Figure 13 illustrates the meridional-vertical cross sections at 125°E for virtual potential temperature and zonal wind from 23 to 26 June at 1200 UTC. It is evident that there is a

strong stable layer existing above 200 hPa and a wide zone of strong zonal wind in the whole troposphere between 27°-40°N. The upper-level jet axes locate where isentropic surfaces branch off to create the Mei-yu front which develops along with the upper-level jets' intensification in the upper troposphere (Fig. 13b,c). At the same time, easterly wind gradually intensifies and expands downwards in accordance with the development of the dewpoint front in the lower troposphere between 21°-25°N. However, the consistence between the intensity of local zonal wind and the intensity of the Mei-yu and dewpoint front is observed. On the last day when the upper-level jets weaken and the isotaches distribute more vertically, the Mei-yu front starts to weaken at this longitude (Fig. 13d).

Figure 14 draws similar sections except for the TEPV and virtual potential temperature. Unsurprisingly, the Mei-yu front does not develop when the TEPV remains weak (Fig. 14a). Afterwards, this term remarkably increases in the frontal zone and leads to the front's development. Also worthy to note that the Mei-yu front's intensity varies with height, depending on the TEPV distribution, and becomes strongest where the local maximum TEPV appears on about 100 hPa beneath the upper-level jet axes (Fig. 14b,c). In the lower troposphere, the TEPV increases between 21°-25°N where the dewpoint front develops as hardly seen. The structural symmetry between the Mei-yu and dewpoint front can be found in the lower troposphere due to the TEPV sign opposite. However, the dewpoint front does not develop with height and is much weaker because the TEPV is confined in the lower troposphere with much smaller magnitudes in the dewpoint front region.

5. Summary and concluding remarks

The Mei-yu front system is a high-impact weather system which is frequently observed in the EASM circulation and plays a key role in water resource management of

the countries where it appears. Despite that, its dynamic formation mechanisms are not well clarified, since it often relates to complicated phenomena owning a wide spectrum of spatial scales, from meso- to synoptic-scale, such as MCSs, lower- and upper-level jets, mesolows, mesohighs, and synoptic-scale lows, etc. To some extent, this multi-scale feature might cause remarkable difficulties to the EASM studies.

For the typical period from 23 to 27 June 1999, the present simulations show that the Mei-yu front system has warm-core structure bounded on the north by the Mei-yu front and on the south by the dewpoint front. The dewpoint front can only be clearly seen under 500 hPa meanwhile the Mei-yu front develops with height. The Mei-yu front strengthens along with the upper-level jets' development and the eastward propagation of the East Asia cold trough, and holds larger thermal deviations from the hydrostatic state in the whole troposphere. In addition to the presence of midlatitude westerly winds along the Mei-yu front, the Mei-yu precipitation is also an original feature showing the independence of the EASM from the South Asia summer monsoon.

Choosing diagnostic tools is essential because it decides if specific mechanisms are dynamically interpreted in the easiest ways. In the present study, the XRV equation is used to diagnose synoptic-scale physical mechanisms associated with the Mei-yu front and indicates that the MGAB is positive in the dewpoint front region and negative along the Mei-yu front. By contrast, the TEPV has opposite sign and represents opposite physical mechanism. In addition, it dominates over the MGAB where the fronts develop and is, therefore, responsible for the formation and evolution of the Mei-yu front system. In other words, the favorable condition for the Mei-yu frontogenesis has stronger TEPV which dramatically tilts isentropic surfaces from south to north in the layers beneath the upper-level jets. Simultaneously, the MGAB resists the TEPV and acts as a predominant frontolysis factor by tilting isentropic surfaces in the opposite direction.

Conducting an auxiliary experiment where the upper-level jets are artificially weakened, the present simulations state that the upper-level jets' development is the direct cause of the Mei-yu front's development, affects the intensity of the East Asia cold trough, and excites mesoscale disturbances propagating downstream. Although the upper-level jets are only weakened in the layer higher than about 500 hPa, however, the impact actually penetrate downwards to 700 hPa, exhibiting that the Mei-yu front's formation is generated at higher levels. As another result of the upper-level jets' development, the "cooling" area is present in the Mei-yu front region at 300 hPa, which extends over a distance of thousands of kilometers across the Korean peninsula and Japan. This could be deduced that whenever the upper-level jets are weakened, the MGAB more stabilizes the atmosphere against the TEPV by lowering isentropic surfaces to the north and lifting them to the south of jets. The stretching effect and the twisting effect of relative vorticity have much minor roles in this case study.

The meridional-vertical cross sections definitely clarify that the Mei-yu front's formation originates from the stable layer located near tropopause, and its required condition is the presence of the upper-level jets within this layer. Strong westerly wind exists in the whole troposphere to create a preferable zone to the Mei-yu front between 27°-40°N. The Mei-yu front's evolution coincides with the development of the TEPV in the frontal zone, starting from the upper-level jets. The downward extension of the upper-level easterly wind exactly agrees with the development of the dewpoint front between 21°-25°N. However, the dewpoint front is much weaker and confined in the lower troposphere where the TEPV is much smaller than in the Mei-yu frontal zone.

Finally, at the Lagrangian ζ point of view, the TEPV contributes as the unique predominant source while the MGAB plays the role of a major sink term. This might be why large-scale fronts could not be formed in the equatorial belt where the planetary

vorticity is nearly equal to zero and the vertical shear of zonal wind is always small. The present simulations also suggest that further diagnostic studies might be necessary to better understand large-scale fronts in winter, which cause severe cold surges in a vast region of the Eurasian continent.

6. Acknowledgments.

This research was supported by the Vietnam's National Foundation for Science and Technology Development (NAFOSTED), and partly supported by the National Science Foundation and the Global Environment Research Project Fund (S-5-3) of the Ministry of the Environment, Japan. NCEP-NCAR Reanalysis data provided by the NOAA-CIRES ESRL/PSD Climate Diagnostics branch, Boulder, Colorado, USA, from their Website at http://www.cdc.noaa.gov/. Weekly sea surface temperature is provided at ftp://ftp.emc.ncep.noaa.gov/cmb/sst/oisst_v2/.

7. References

Bluestein, H. B., 1993: *Synoptic-dynamic meteorology in midlatitudes*. Vol. 2. Oxford University Press, 594 pp.

Chang, C.-P., L. Yi, and G. T.-J. Chen, 2000: A numerical simulation of vortex development during the 1992 East Asian summer monsoon onset using the Navy's regional model. *Mon. Wea. Rev.*, **128**, 1604-1631.

Chen, G. T.-J., and C.-P. Chang, 1980: The structure and vorticity budget of an early summer monsoon trough (Mei-Yu) over southeastern China and Japan. *Mon. Wea. Rev.*, **108**, 942-953.

Chen, G. T.-J., C.-C. Wang, and S.-W. Chang, 2008: A diagnostic case study of Mei-yu frontogenesis and development of wavelike frontal disturbances in the subtropical environment. *Mon. Wea. Rev.*, **136**, 41-61.

Chen, G. T.-J., C.-C. Wang, and L.-F. Lin, 2006: A diagnostic study of a retreating Mei-yu front and the accompanying low-level jet formation and intensification. *Mon. Wea. Rev.*, **134**, 874-896.

Chen, G. T.-J., C.-C. Wang, and S.C-S. Liu, 2003: Potential vorticity diagnostics of a Mei-yu front case. *Mon. Wea. Rev.*, **131**, 2680-2696.

Chen, G. T.-J., C.-C. Wang, and A.-S. Wang, 2007: A case study of subtropical frontogenesis during a blocking event. *Mon. Wea. Rev.*, **135**, 2588-2609.

Chien, F.-C., Y.-H. Kuo, and M.-J. Yang, 2002: Precipitation forecast of MM5 in the Taiwan area during the 1998 Mei-yu season. *Wea. Forecasting*, **17**, 739-754.

Cho, H.-R., and G. T.-J. Chen, 1995: Mei-yu frontogenesis. *J. Atmos. Sci.*, **52**, 2109-2120.

Holton, J. R., 2004: *An introduction to dynamic meteorology*. 4th Edition. Academic Press, 535 pp.

Jung, J.-H., and A. Arakawa, 2008: A three-dimensional anelastic model based on the

vorticity equation. *Mon. Wea. Rev.*, **136**, 276-294.

Kalnay, E., and Coauthors, 1996: The NCEP/NCAR 40-year reanalysis project. *Bull. Amer. Meteor. Soc.*, **77**, 437-471.

Kawatani, Y., and M. Takahashi, 2003: Simulation of the Baiu front in a High Resolution AGCM. *J. Meteor. Soc. Japan*, **81**, 113-126.

Lau, K.-M., G. J. Yang, and S.H. Shen, 1988: Seasonal and intraseasonal climatology of summer monsoon rainfall over East Asia. *Mon. Wea. Rev.*, **116**, 18-37.

Ninomiya, K., and Y. Shibagaki, 2007: Multi-scale features of the Meiyu-Baiu front and associated precipitation systems. *J. Meteor. Soc. Japan*, **85**, 103-122.

Qian, J.-H., W.-K. Tao, and K.-M. Lau, 2004: Mechanisms for torrential rain associated with the Mei-yu development during SCSMEX 1998. *Mon. Wea. Rev.*, **132**, 3-27.

Reynolds, R. W., N. A. Rayner, T. M. Smith, D. C. Stokes, and W. Wang, 2002: An improved in situ and satellite SST analysis for climate. *J. Climate*, **15**, 1609-1625.

Sampe, T., and S-P. Xie, 2010: Large-scale dynamics of the Meiyu-Baiu rainband: Environmental forcing by the westerly jet. *J. Climate*, **23**, 113-134.

Shen, X., M. Kimoto, A. Sumi, A. Numaguti, and J. Matsumoto, 2001: Simulation of the 1998 East Asian summer monsoon by the CCSR/NIES AGCM. *J. Meteor. Soc. Japan*, **79**, 741-757.

Shibagaki, Y., and K. Ninomiya, 2005: Multi-scale interaction processes associated with development of a sub-synoptic-scale depression on the Meiyu-Baiu frontal zone. *J. Meteor. Soc. Japan*, **83**, 219-236.

Truong, N. M., T. T. Tien, R. A. Pielke Sr., C. L. Castro, and G. Leoncini, 2009: A modified Kain-Fritsch scheme and its application for simulation of an extreme precipitation event in Vietnam. *Mon. Wea. Rev.*, **137**, 766-789.

Walko, R. L., W. R. Cotton, M. P. Meyers, and J. Y. Harrington, 1995: New RAMS cloud

microphysics parameterization. Part I: The single moment scheme. *Atmos. Res*., **38**, 29-62.

Wang, B., 1987: The development mechanism for Tibetan Plateau warm vortices. *J. Atmos. Sci.*, **44**, 2978-2994.

Wang, Y., O. L. Sen, and B. Wang, 2003: A highly resolved regional climate model (IPRC-RegCM) and its simulation of the 1998 severe precipitation event over China. Part I: Model description and verification of simulation. *J. Climate*, **16**, 1721-1738.

Yanai, M., and G-X. Wu, 2006: Effects of the Tibetan plateau. *The Asian monsoon, Springer*. Praxis Publishing, 513-549.

Yihui, D., and J. C. L. Chan, 2005: The East Asian summer monsoon: An overview. *Meteorol. Atmos. Phys.*, **89**, 117–142.

Yoshikane, T., F. Kimura, and S. Emori, 2001: Numerical study on the Baiu front genesis by heating contrast between land and ocean. *J. Meteor. Soc. Japan*, **79**, 671-686.

Zhang, Q.-H., K.-H. Lau, Y.-H. Kuo, and S.-J. Chen, 2003: A numerical study of a mesoscale convective system over the Taiwan strait. *Mon. Wea. Rev*., **131**, 1150-1170.

Zhou, Y., S. Gao, and S. S. P Shen, 2004: A diagnostic study of formation and structures of the Meiyu front system over East Asia. *J. Meteor. Soc. Japan*, **82**, 1565-1576.

8. Figure captions

Figure 1: Schematic description for the 3-D interaction between the twisting effect of the planetary vorticity and meridional gradient of the atmospheric buoyancy in the environment of strong vertical shear of zonal wind.

Figure 2: Domain and model topography in m above MSL.

Figure 3: Simulated virtual potential temperature and wind vector at 700 hPa on 23 (a), 24 (b), 25 (c), and 26 (d) June 1999 at 1200 UTC. Contour interval is 1°K, and model topography higher than 3000 m above MSL is blanked.

Figure 4: Same as Fig. 3 except at 300 hPa. Contour interval is 1.5°K.

Figure 5: Total rainfall accumulated for 24 (a), 48 (b), 72 (c), and 96 (d) h model integration, starting from 0000 UTC 23 June 1999.

Figure 6: Meridional gradient of the atmospheric buoyancy at 700 hPa on 23 (a), 24 (b), 25 (c), and 26 (d) June 1999 at 1200 UTC. Positive contours are solid and zero lines are omitted. Contour interval is 3×10^{-7} s^{-1}, and model topography higher than 3000 m above MSL is blanked.

Figure 7: Same as Fig. 6 except for the twisting effect of the planetary vorticity. Negative contours are solid and zero lines are omitted.

Figure 8: Meridional gradient of the atmospheric buoyancy at 300 hPa on 23 (a), 24 (b), 25 (c), and 26 (d) June 1999 at 1200 UTC. Positive contours are solid and zero lines are omitted, contour interval is 3×10^{-7} s^{-1}.

Figure 9: Same as Fig. 8 except for the twisting effect of the planetary vorticity. Negative contours are solid and zero lines are omitted.

Figure 10: Same as Fig. 4 except upper-level jets are weakened by Eq. (4).

Figure 11: Difference in 300-hPa virtual potential temperature between the Ctrl and Jmod experiment on 23 (a), 24 (b), 25 (c), and 26 (d) June 1999 at 1200 UTC. Negative contours

are dashed and zero lines are omitted, contour interval is 1°K.

Figure 12: Same as Fig. 11 except at 700 hPa.

Figure 13: Meridional-vertical cross sections at 125°E for virtual potential temperature (thin solid contours) and zonal wind (positive contours are dashed) on 23 (a), 24 (b), 25 (c), and 26 (d) June 1999 at 1200 UTC. Contour intervals are 3°K and 5 m s^{-1}, respectively.

Figure 14: Same as Fig. 13 except for virtual potential temperature and the twisting effect of the planetary vorticity. Contour intervals are 3°K and 1.5×10^{-7} s^{-1}, respectively.

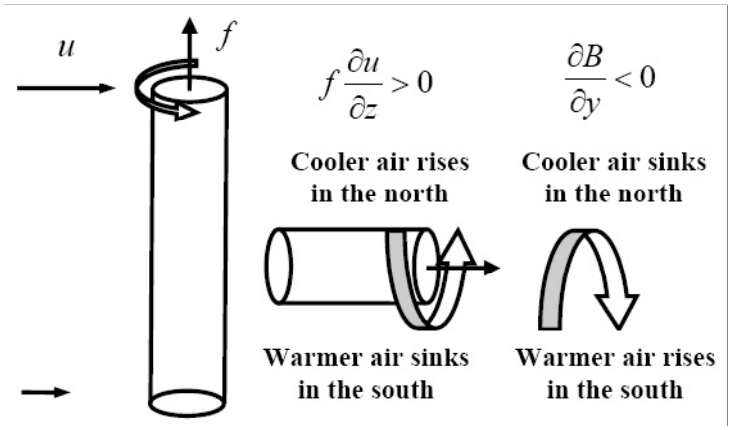

Figure 1: Schematic description for the 3-D interaction between the twisting effect of the planetary vorticity and meridional gradient of the atmospheric buoyancy in the environment of strong vertical shear of zonal wind.

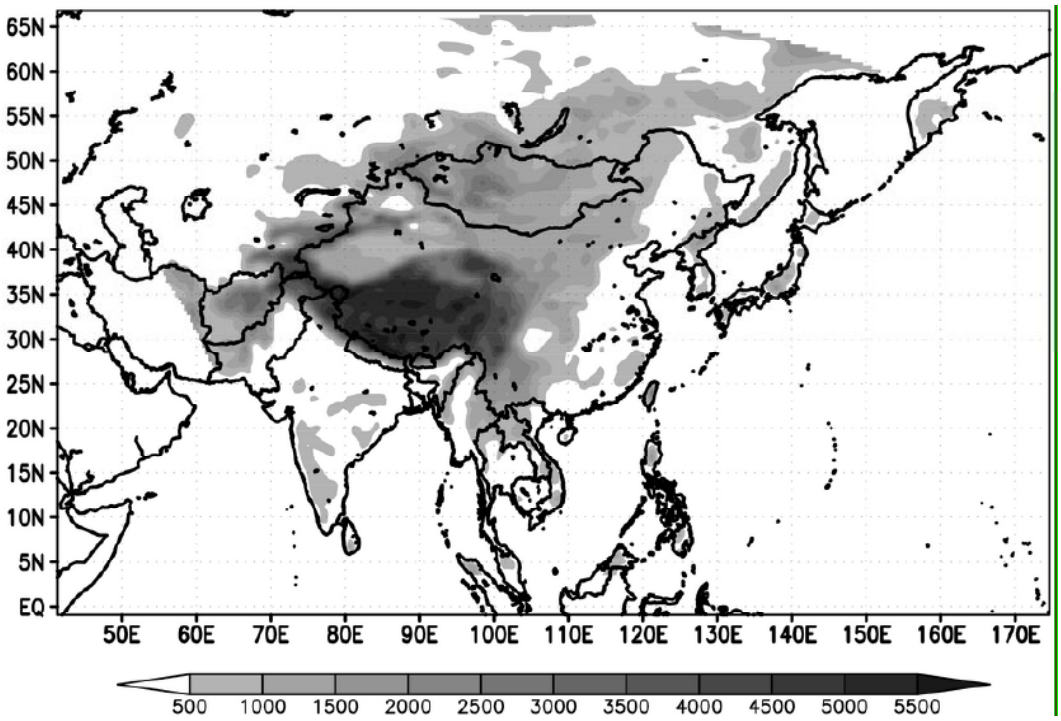

Figure 2: Domain and model topography in m above MSL.

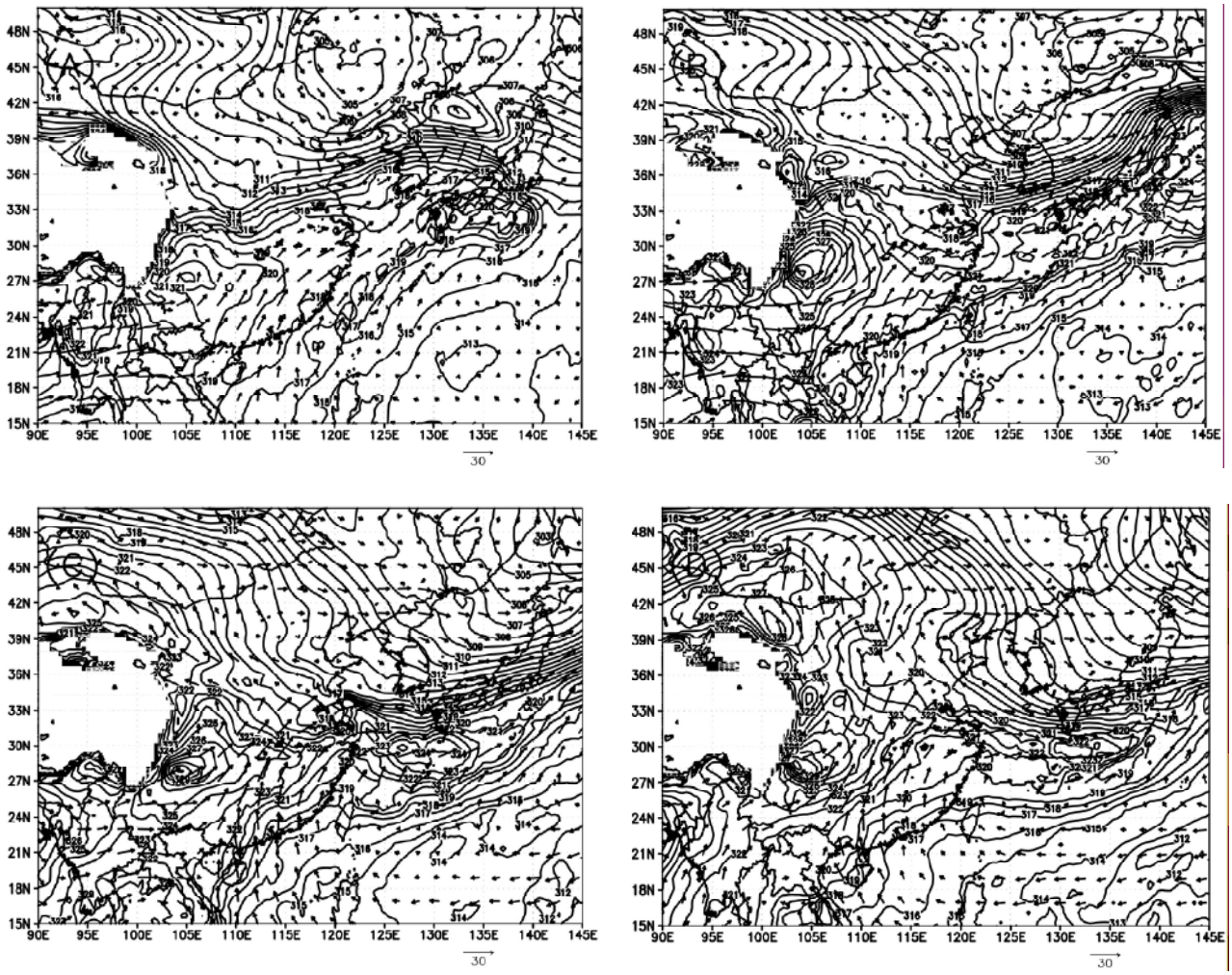

Figure 3: Simulated virtual potential temperature and wind vector at 700 hPa on 23 (a), 24 (b), 25 (c), and 26 (d) June 1999 at 1200 UTC. Contour interval is 1°K, and model topography higher than 3000 m above MSL is blanked.

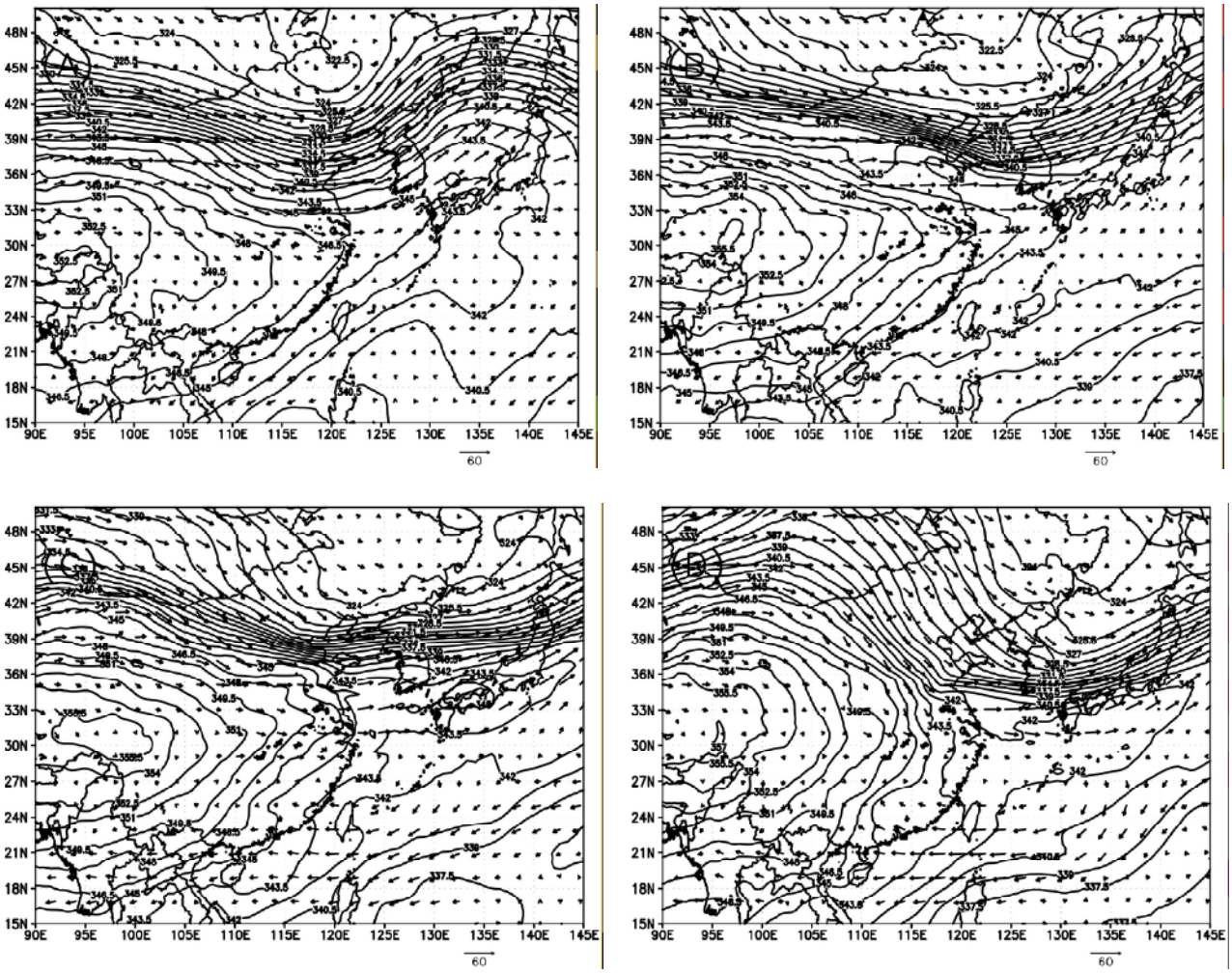

Figure 4: Same as Fig. 3 except at 300 hPa. Contour interval is 1.5°K.

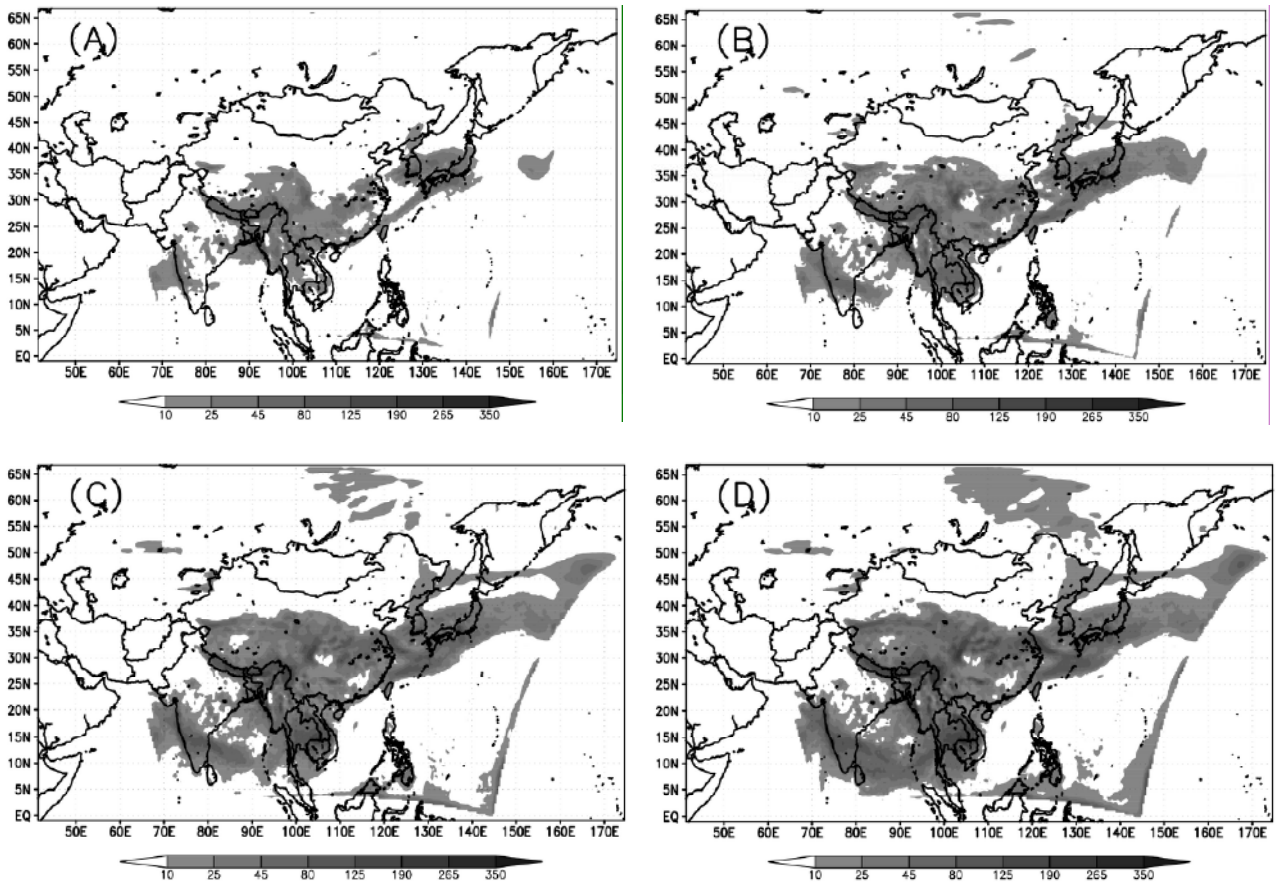

Figure 5: Total rainfall accumulated for 24 (a), 48 (b), 72 (c), and 96 (d) h model integration, starting from 0000 UTC 23 June 1999.

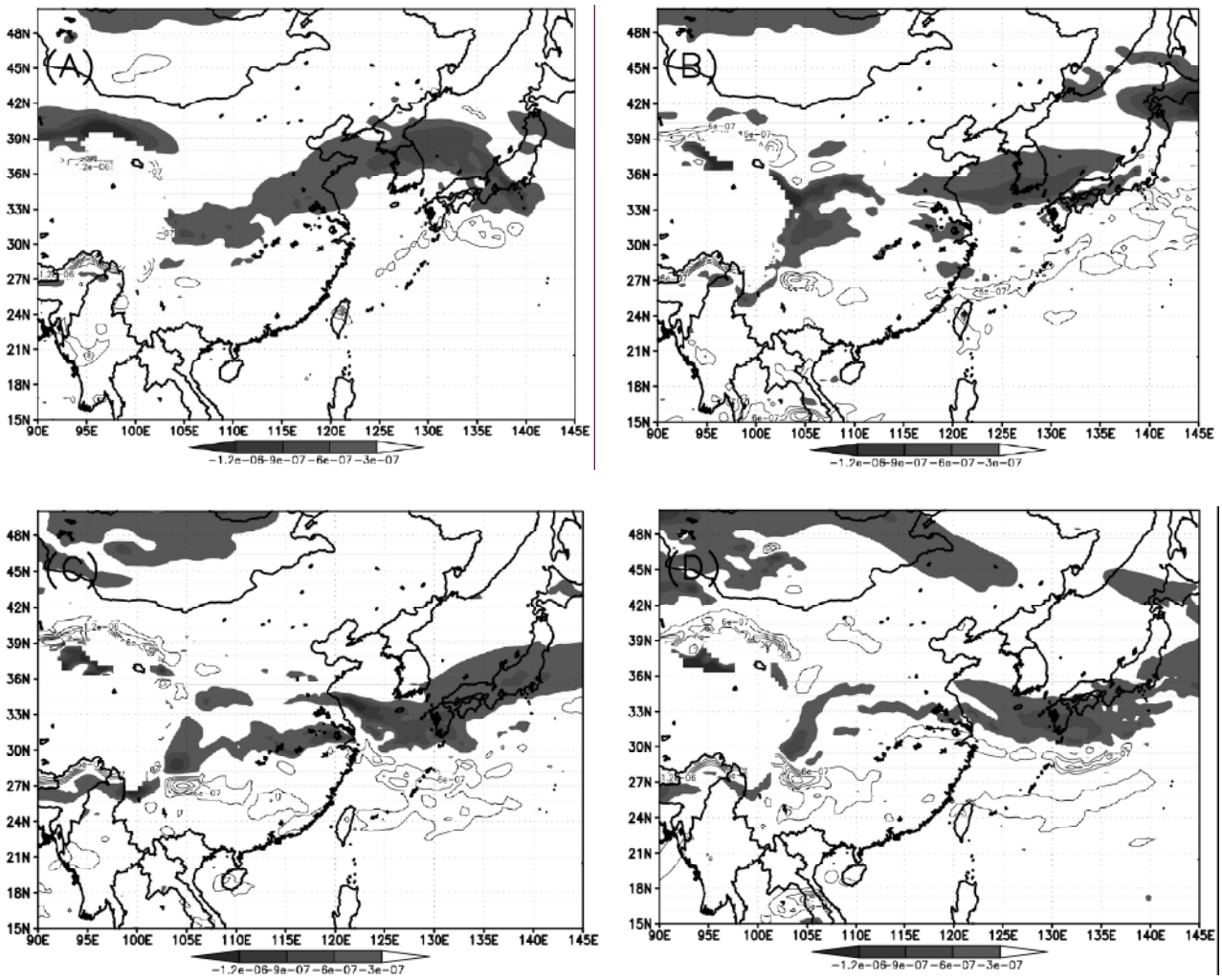

Figure 6: Meridional gradient of the atmospheric buoyancy at 700 hPa on 23 (a), 24 (b), 25 (c), and 26 (d) June 1999 at 1200 UTC. Positive contours are solid and zero lines are omitted. Contour interval is 3×10^{-7} s^{-1}, and model topography higher than 3000 m above MSL is blanked.

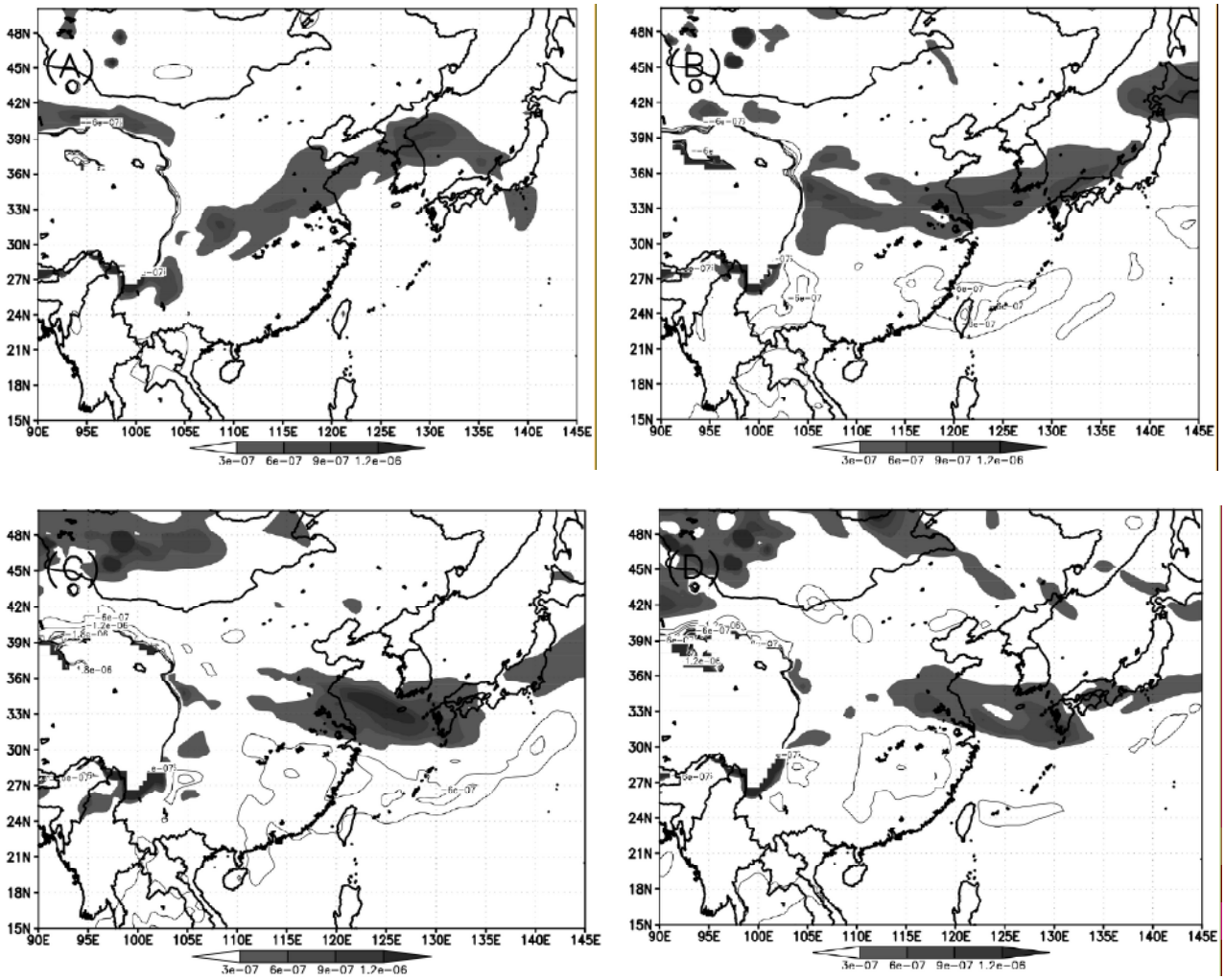

Figure 7: Same as Fig. 6 except for the twisting effect of the planetary vorticity. Negative contours are solid and zero lines are omitted.

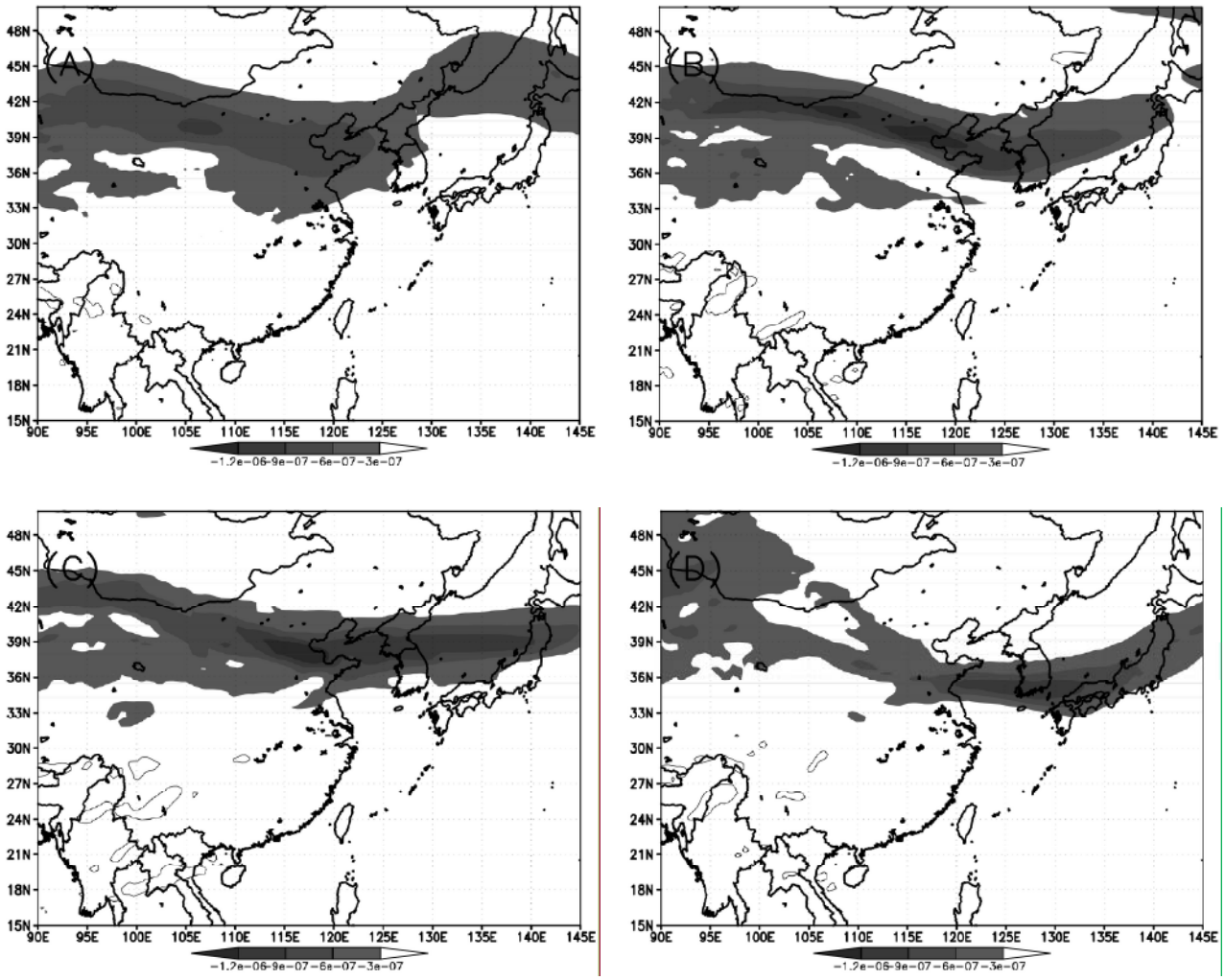

Figure 8: Meridional gradient of the atmospheric buoyancy at 300 hPa on 23 (a), 24 (b), 25 (c), and 26 (d) June 1999 at 1200 UTC. Positive contours are solid and zero lines are omitted, contour interval is 3×10^{-7} s^{-1}.

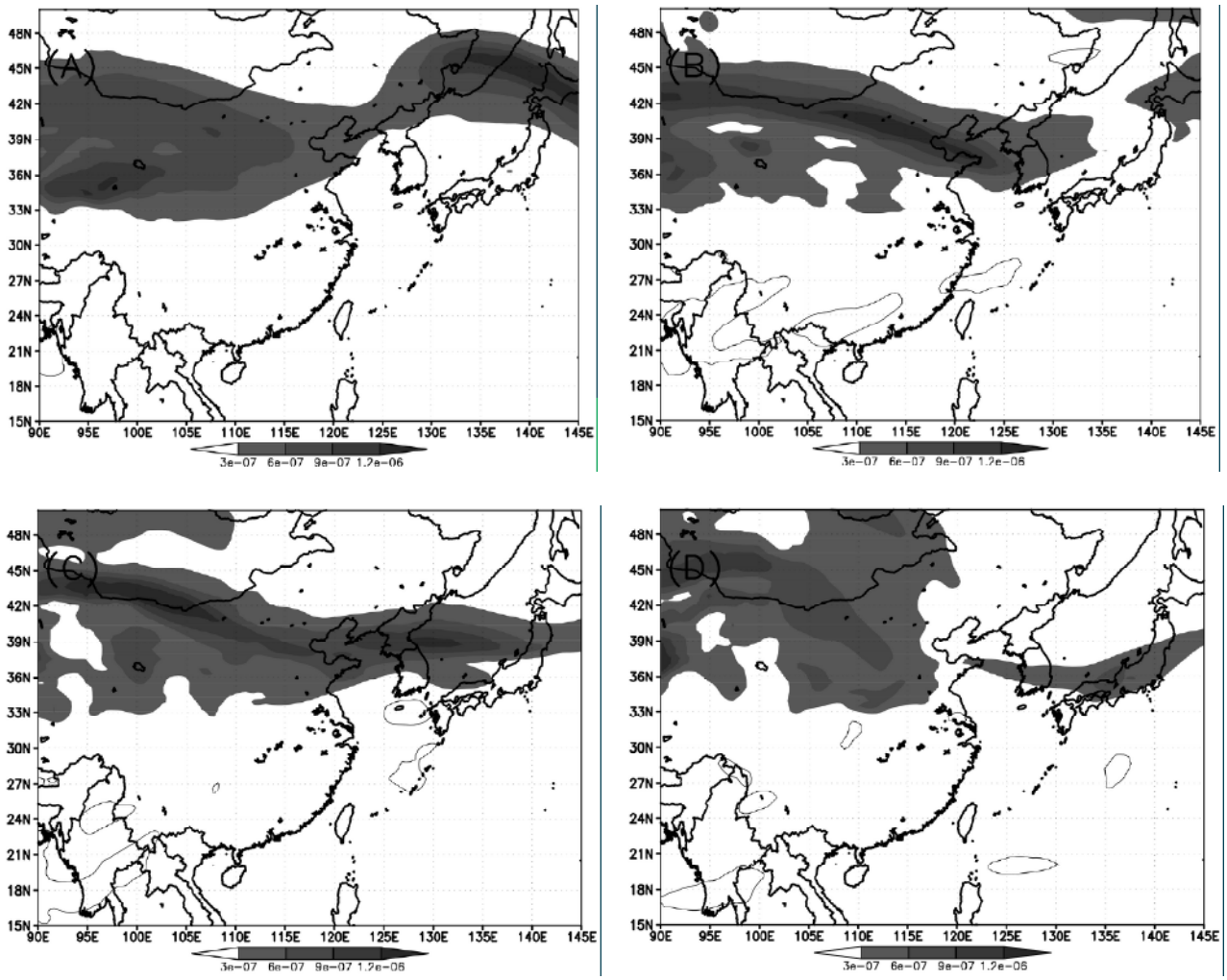

Figure 9: Same as Fig. 8 except for the twisting effect of the planetary vorticity. Negative contours are solid and zero lines are omitted.

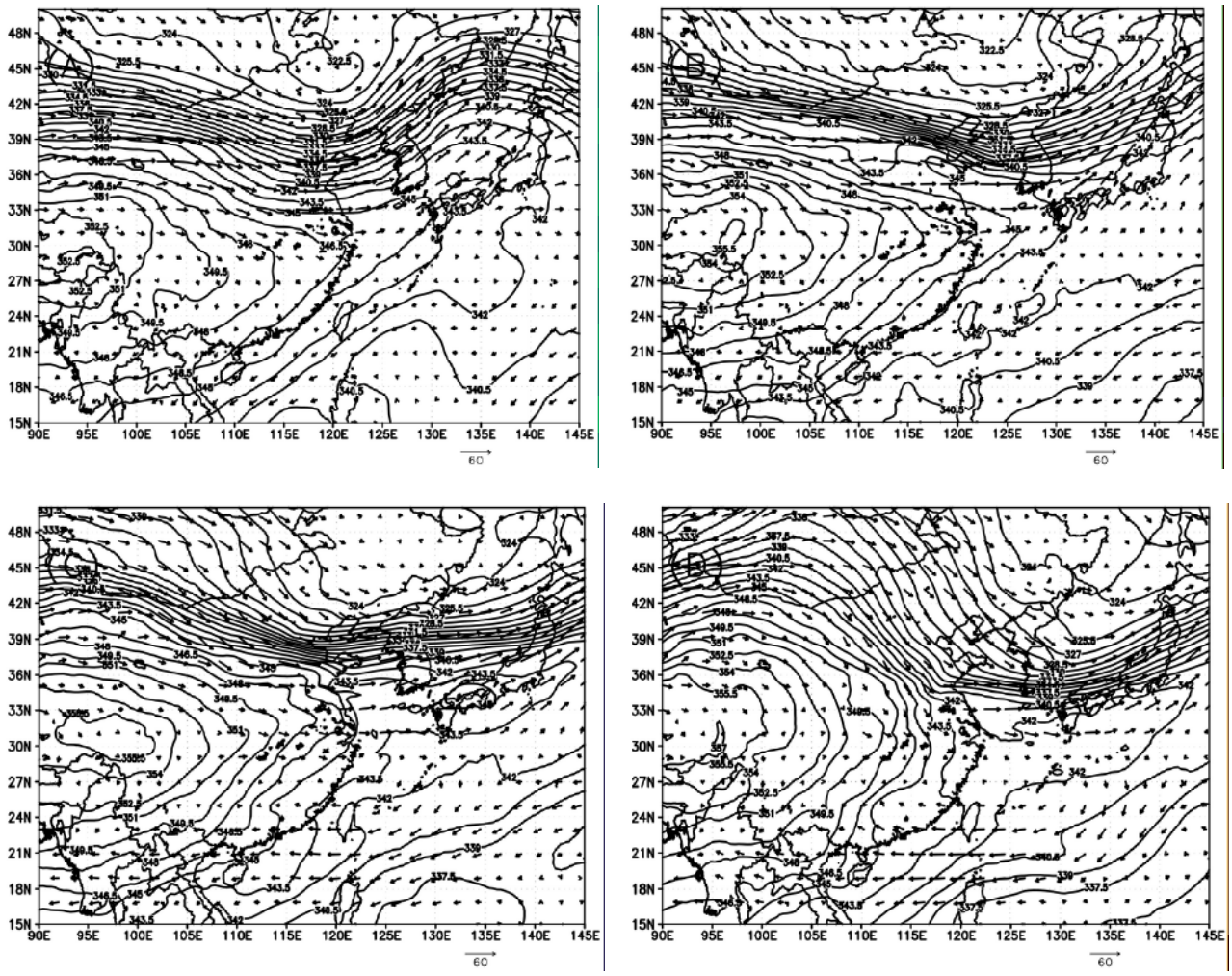

Figure 10: Same as Fig. 4 except upper-level jets are weakened by Eq. (4).

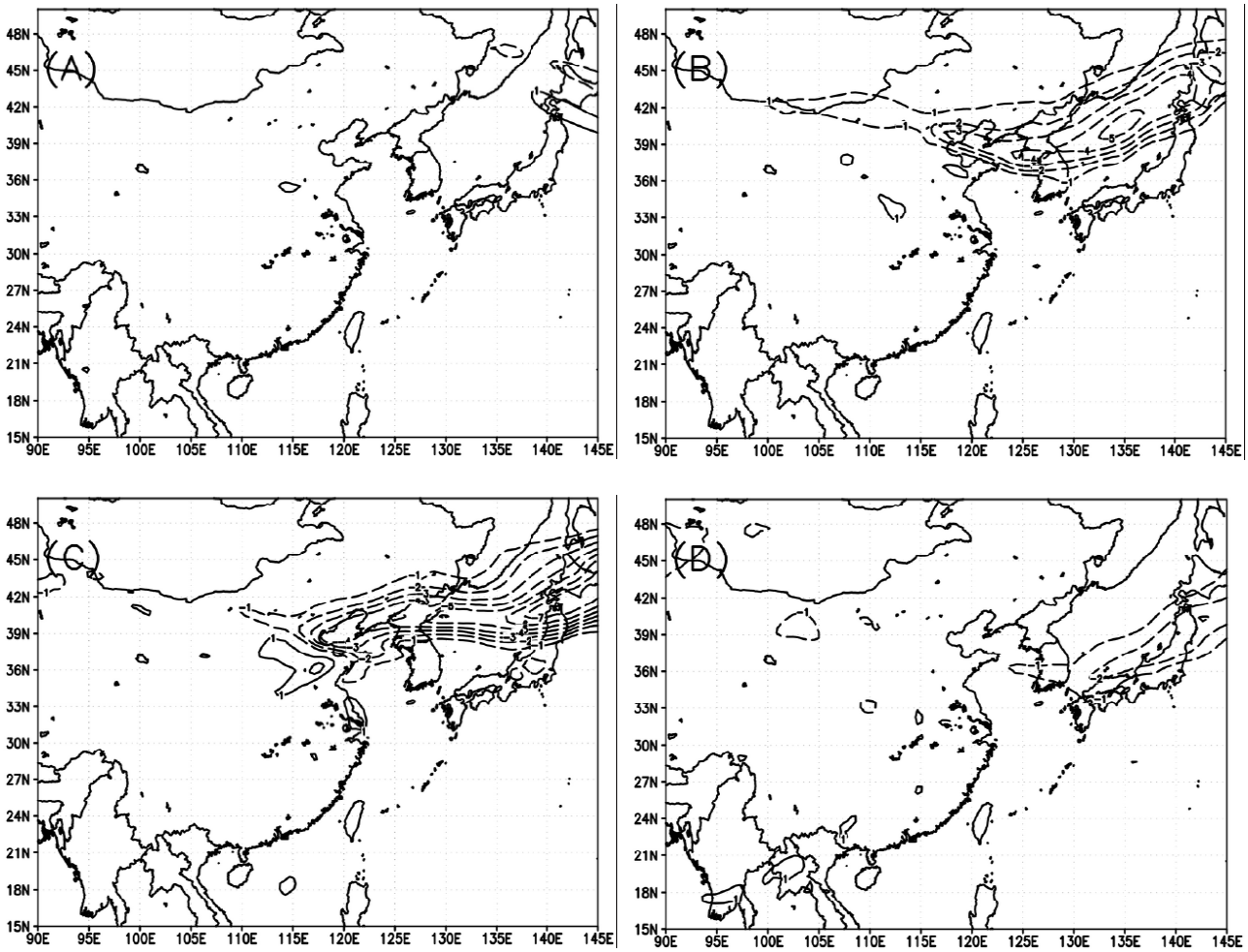

Figure 11: Difference in 300-hPa virtual potential temperature between the Ctrl and Jmod experiment on 23 (a), 24 (b), 25 (c), and 26 (d) June 1999 at 1200 UTC. Negative contours are dashed and zero lines are omitted, contour interval is 1°K.

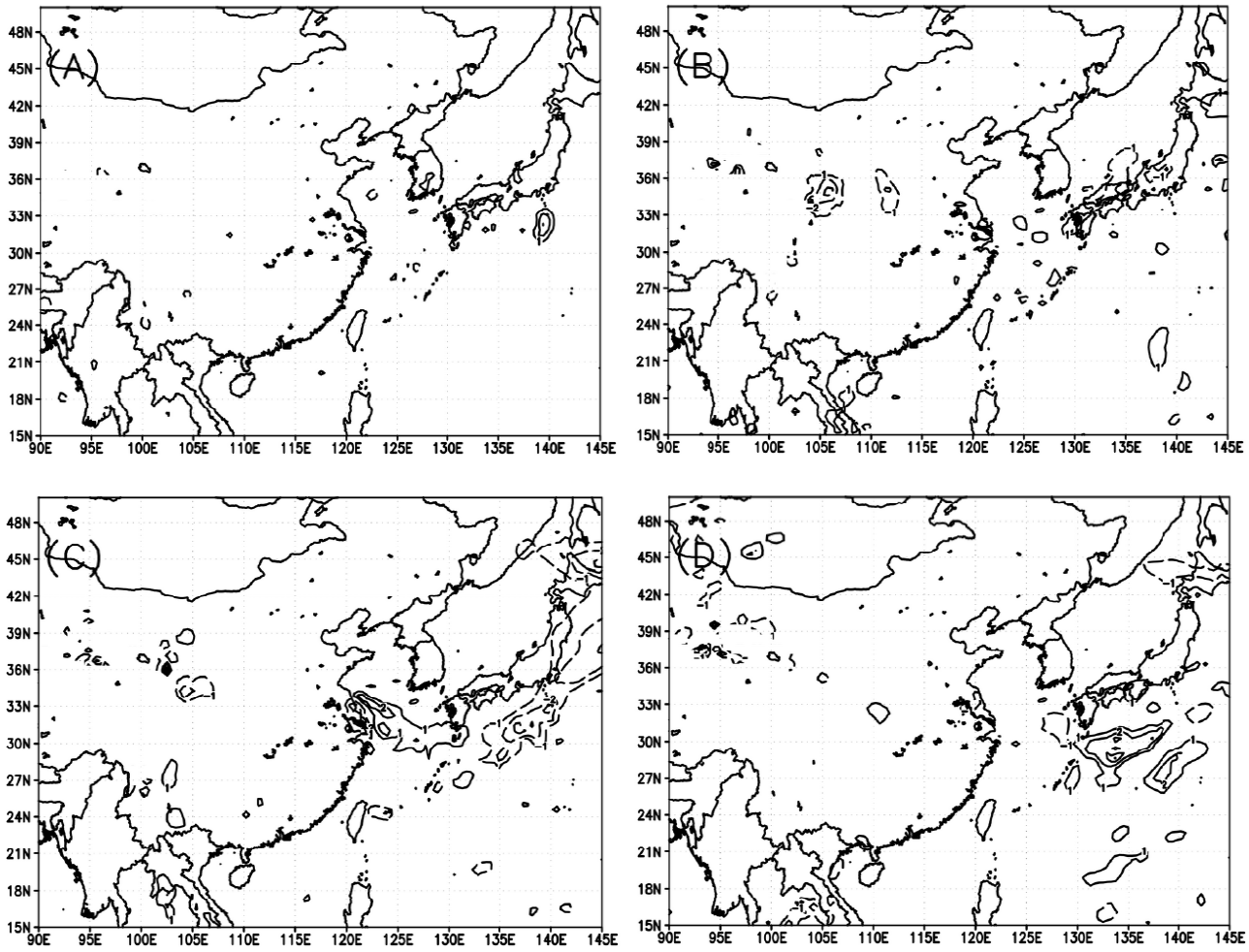

Figure 12: Same as Fig. 11 except at 700 hPa.

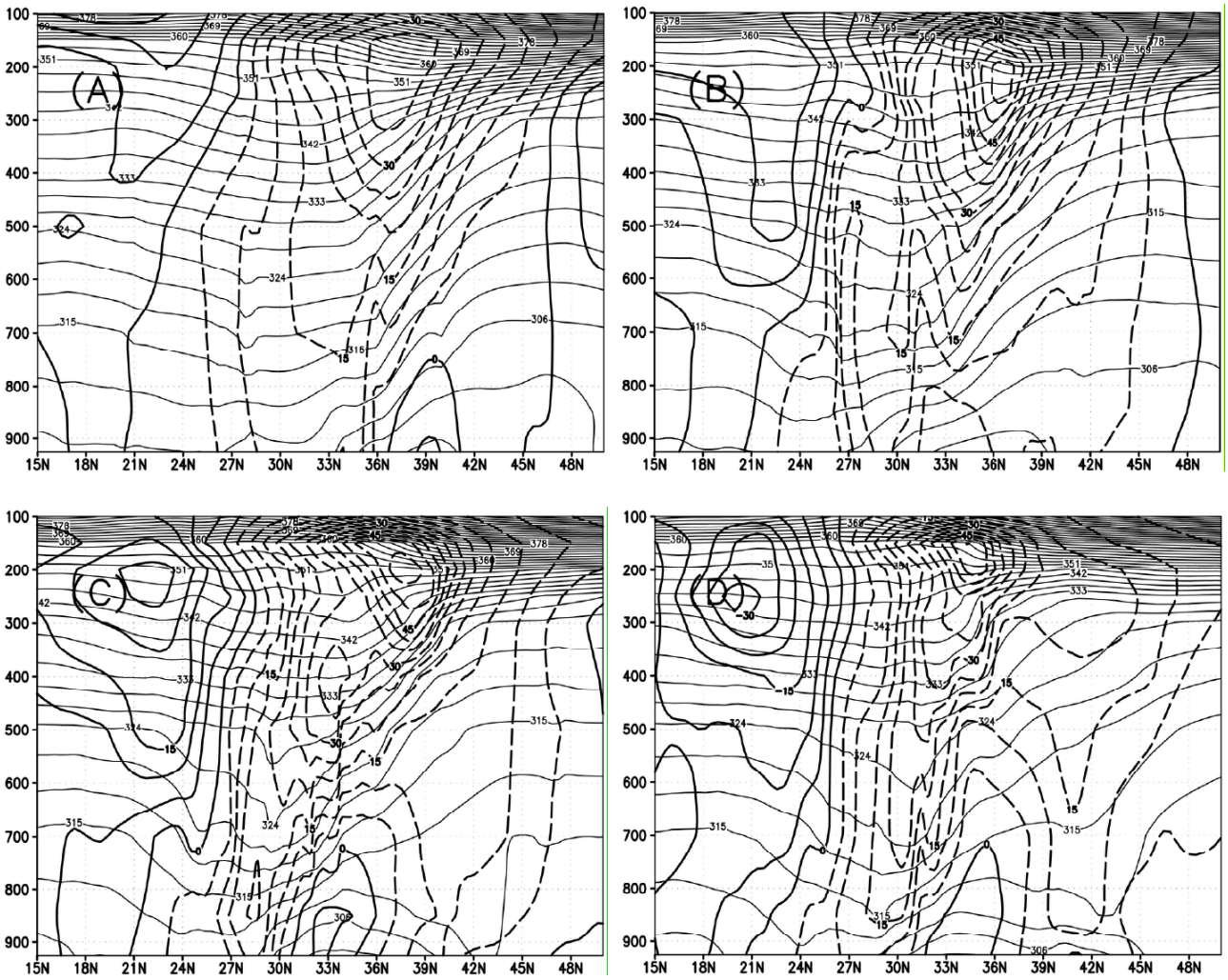

Figure 13: Meridional-vertical cross sections at 125°E for virtual potential temperature (thin solid contours) and zonal wind (positive contours are dashed) on 23 (a), 24 (b), 25 (c), and 26 (d) June 1999 at 1200 UTC. Contour intervals are 3°K and 5 m s^{-1}, respectively.

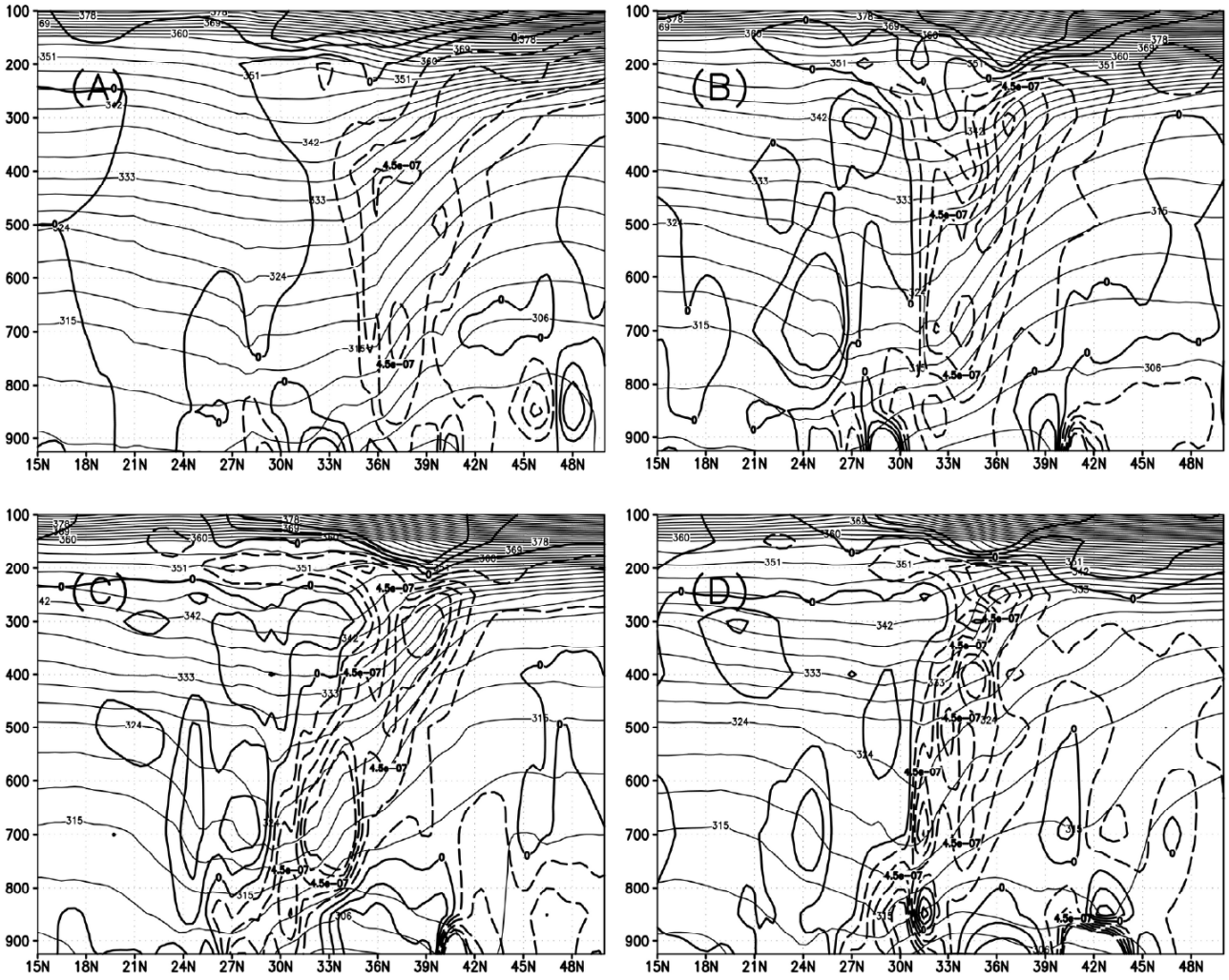

Figure 14: Same as Fig. 13 except for virtual potential temperature and the twisting effect of the planetary vorticity. Contour intervals are 3°K and 1.5×10^{-7} s^{-1}, respectively.

TABLE 1. Model configuration and experiments where jet-modification run is described in Section 4.

Exp.	Grid domain	Grid center	Grid spacing	Vertical levels	Jet modification
Ctrl	207 × 161	35°N-108°E	45 km	30	No
Jmod					Yes

TABLE 2. Common magnitudes of the terms in the XRV equation.

Term	TEPV	MGAB	TERV	SERV
Magnitude	6.E-7÷1.2E-6	3.E-7÷9.E-7	<<3.E-7	<<3.E-7